Fatigue Tests of Prestressed Concrete Pavements

A. P. CHRISTENSEN and B. E. COLLEY, Paving Development Section, Portland Cement Association, Skokie, Illinois

The fatigue characteristics of prestressed concrete pavements were studied by repetitive moving load tests on 16 reduced scale prestressed concrete slabs. Each slab was 16 ft long, 12 ft wide, and 1 in. thick. Variables were magnitude of load, amount of longitudinal and transverse prestress, and subgrade strength.

Relationships were established between load magnitude, prestressed pavement properties, and the number of load coverages causing failure. Data from tests on slabs with varying magnitudes of prestress indicate that a minimum prestress of approximately 30 psi in both longitudinal and transverse directions is required to avoid top surface cracking when relatively few moving loads greater than those causing bottom surface cracking are applied repeatedly at interior locations. Data from tests on slabs cast on foundations of different strengths indicated that an increase in the foundation strength resulted in an increase in the number of load coverages causing failure.

•THE LOAD response of prestressed concrete pavements is being studied at the Research and Development Laboratories of the Portland Cement Association. The first published result of this study was a theoretical procedure (1) for determining the magnitude and distribution of stresses and deflections in prestressed concrete pavements for loads beyond cracking of the bottom surface. This procedure is specifically applicable to a centrally loaded infinite slab supported by a "dense liquid" foundation and prestressed equally in longitudinal and transverse directions.

To test the validity of the assumptions made in the theoretical procedure, load tests (2) were conducted on three reduced scale prestressed concrete slabs supported on a coil spring subgrade. Measurements of strain and deflection were made at a number of locations and load increments. Comparisons between test data and theory indicated fair agreement for values of deflection; however, measured strains were significantly smaller than those predicted by theory. The theoretical assumption that the moment-curvature relationship can be represented by two straight lines, an elastic portion with a constant slope followed by a plastic portion in which curvature increases under constant moment, was shown to be conservative for the static type of loading used.

Strain and deflection data were also reported (3) from static load tests conducted on three concrete slabs post-tensioned with steel strands. Each slab was 30 ft long, 12 ft wide, and 5 in. thick. Results again indicated that a prestressed concrete pavement can adequately support an edge or interior load of greater magnitude than that causing bottom surface cracking. Crack patterns were similar to those predicted by the theoretical procedure. Bottom surface cracks extended radially from the center of the load; top surface cracks were approximately circular for interior loads and semicircular for edge loads. However, applications of repeated moving loads cause the development of a random pattern of bottom surface cracks. To obtain information on the fatigue characteristics of prestressed concrete pavements with numerous working bottom surface cracks, a program of repetitive moving load tests was initiated on reduced scale prestressed concrete slabs.

Paper sponsored by Committee on Rigid Pavement Design and presented at the 47th Annual Meeting.

SCOPE AND OBJECTIVES

The test program was designed to study the behavior of 16 prestressed concrete slabs subjected to repetitive moving loads. Variables were magnitude of load, amount of longitudinal and transverse prestress, and subgrade strength. Because it was necessary to test a number of slabs to obtain sufficient data for a fatigue diagram, a reduced scale size was selected for the test slabs and the loading apparatus. The slabs were pretensioned and cast in place on either a clay subgrade, granular subbase, or cement-treated subbase.

The specific objectives of the program were (a) to determine a relationship between the load magnitude and the number of coverages causing pavement failure, (b) to determine the influence of prestress magnitude and foundation strength on fatigue properties of prestressed pavements, and (c) to observe the characteristics of a prestressed pavement failure and determine the factors that cause its development.

TEST FACILITIES AND MATERIALS

Data are reported from load tests on 16 concrete slabs 16 ft long, 12 ft wide, and 1 in. thick. Prestressing was accomplished with pretensioned high-strength steel wire. The slabs were cast in place and tested with a moving load apparatus designed for this program.

Test Area, Subgrade, and Subbase Materials

The prestressed slabs were cast and tested in the area shown in Figure 1. This area is enclosed in a 24-ft wide concrete building equipped with thermostatically controlled heaters to provide uniform temperature during the heating season. The test area was excavated 4 ft below grade to the bottom of the wall footings, and a 5-in. reinforced concrete floor was cast to form an enclosure for a subgrade material. A waterproofing compound was applied to the floor and walls to protect the subgrade from moisture changes. A clay material was compacted into this enclosure to a depth of 4 ft. Properties of the clay subgrade are given in Table 1. The modulus of subgrade reaction, k, is given in Table 5. It will be shown later that the average radius of relative stiffness for the 16 test slabs was 7.3 in. Therefore the subgrade depth was 6.6 times the radius of relative stiffness, and behavior should approximate a subgrade of infinite depth. The radius of relative stiffness, L, is a ratio of the stiffness of the slab to the stiffness of the subgrade (Eq. 3).

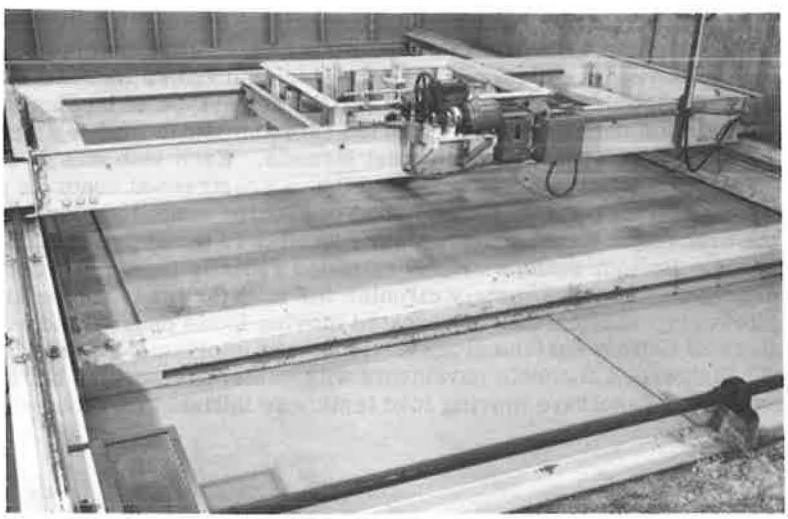

Figure 1. Test area and moving load apparatus.

TABLE 1

SUBGRADE PROPERTIES

Property	Particle Size (mm)	Percent	PCF
Material			
Gravel	76.2 -2.0	0	–
Coarse sand	2.0 -0.42	6	–
Fine sand	0.42 -0.074	8	–
Silt	0.074-0.005	48	–
Clay	smaller than 0.005	38	–
Liquid limit		36	–
Plasticity index		19	–
Maximum dry density (AASHO standard)		–	112
Optimum moisture		16	–

TABLE 2

SUBBASE PROPERTIES

Property	Particle Size (mm)	Percent	PCF
Granular Material			
Gravel	76.2 -2.0	46	–
Coarse sand	2.0 -0.42	24	–
Fine sand	0.42 -0.074	17	–
Silt	0.074-0.005	10	–
Clay	smaller than 0.005	3	–
Plasticity index		0	–
Maximum dry density (AASHO standard)		–	141
Optimum moisture		7	–
Cement-Treated Material			
Gravel	76.2 -2.0	27	–
Coarse sand	2.0 -0.42	23	–
Fine sand	0.42 -0.074	32	–
Silt	0.074-0.005	16	–
Clay	smaller than 0.005	2	–
Plasticity index		0	–
Maximum dry density (AASHO standard)		–	125
Optimum moisture		10	–
Cement content		5.5	–

Thirteen of the test slabs were cast on the clay subgrade without a subbase layer. The top surface of the clay was carefully finished to grade with a metal screed to obtain a level casting surface for uniform slab depth. After leveling, the subgrade was covered with two sheets of 4-mil thick polyethylene to retain moisture in the clay subgrade and to reduce stresses resulting from restraint to horizontal slab movement. The clay subgrade was removed to a depth of about 1 ft after each test and the soil was pulverized, reworked to optimum, and recompacted.

A 6-in. granular subbase was used under two of the test slabs, and a 6-in. cement-treated subbase was used under another. The properties of these subbases are given in Table 2. The modulus of subgrade reaction, k, is given in Table 5. For these tests the top 6 in. of clay subgrade was removed and replaced with subbase material. Polyethylene sheets were placed between the subbase and the concrete.

Prestressing

Test slabs were prestressed by the pretensioning method, i.e., the wires were tensioned prior to placing the concrete. After the concrete had attained sufficient strength,

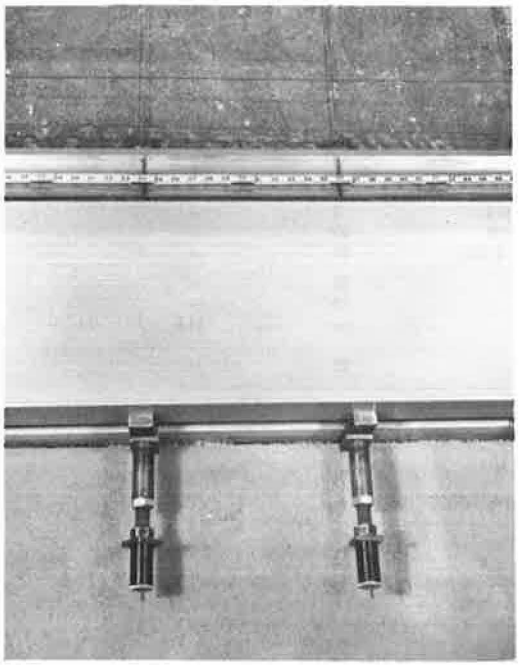

Figure 2. Devices used for tensioning the steel wires.

the wires were released and stress was transferred to the concrete through bond.

Uncoated, stress-relieved No. 12 steel wire was used for applying prestress at the mid-depth of the slabs. Wires in one direction alternated above and below those extending at right angles. The wire diameter was 0.1055 in., area 0.00875 sq. in., modulus of elasticity 27, 600, 000 psi, and ultimate strength 260, 000 psi.

The reaction frame used for tensioning the wires had inside dimensions of 14 by 17 ft. Each side of the frame was formed by a pair of 15-in. steel channels between which the wires were inserted. Bolted moment connections were used at the frame corners. Concrete beams resting on the clay subgrade supported the reaction frame in a horizontal plane at the proper elevation for tensioning the wires at slab mid-depth.

Each prestressing wire was tensioned individually by the extension of a telescoping threaded spacer placed between the wire anchor and the reaction frame (Fig. 2). The force in the wire was measured by a transducer (4) placed between the wire anchor and the reaction frame at the side opposite the spacer. After tensioning the wires, a minimum of one day was allowed before casting the concrete slab. The force in each wire was checked and, if necessary, adjusted to the selected magnitude prior to casting.

To insure full prestress near the slab edges, a 1-in. split steel cube was fastened to each wire at the point where the wire entered the steel side forms. The two halves of the cube were grooved slightly undersize for the wire used and were clamped on the wire by countersunk machine screws.

Casting of Concrete

The cement factor of the concrete was 7.0 sk/cu yd; water-cement ratio was 0.52 by weight, and the sand-aggregate ratio was 0.59 by weight. Type 3 cement was used to obtain a high early strength, and the maximum size of gravel aggregate was $\frac{3}{8}$ in. The slump averaged 4.7 in. and vinsol resin was added to provide an average air content of 6.9 percent. Concrete was compacted with a vibrating screed.

After casting, each slab was covered with polyethylene sheeting. The next day, approximately 16 hours later, the sheeting was removed and the top slab surface was coated with a curing compound to reduce moisture losses and thereby minimize curling. Prestressing wires were released after the concrete had cured for 7 days.

Beam specimens 1 by 4 by 22 in. were made at the time of casting from samples of concrete placed in the center portion of each test slab. The beams were cured in a 70 F, 100 percent relative humidity room until tested in flexure with third-point loading on a span of 12 in. It was usually possible to obtain two flexural tests from each beam. A minimum of nine beams was tested for each slab, including three tested when repetitive slab loading was started and three when each failure occurred. Repetitive load tests were started 12 to 14 days after casting. Duration of each test depended on the number of loadings necessary to cause failure and averaged 13 calendar days for all slabs. During the test period, there was relatively little change in the flexural strength of each slab; average values are given in Table 3.

TABLE 3
CONCRETE FLEXURAL STRENGTH

Slab No.	Modulus of Rupture (psi)	Slab No.	Modulus of Rupture (psi)
1	970	9	966
2	880	10	957
3	882	11	970
4	897	12	952
5	952	13	930
6	905	14	963
7	890	15	936
8	916	16	927

A limited number of beams were instrumented with two SR-4 type A9-4 (2-in. length) strain gages on the bottom surface between the third-point loads. Strain measurements during flexural testing of these beams indicated that the average modulus of elasticity for the test slabs was 4, 100, 000 psi.

Load Apparatus

A special load apparatus was constructed for applying repetitive moving loads to the prestressed concrete test slabs. The load apparatus was not designed to simulate traffic operations but rather to develop a random pattern of bottom surface cracks at the interior of each slab. Loads were applied through a single wheel traveling in a number of wheel paths over an interior area 32 in. wide (including the width of the wheel) by 98 in. long. The distances between the loading area and the longitudinal and transverse edges of the 12 by 16-ft slabs were 56 and 47 in. respectively. These edge distances were 7.7 and 6.4 times the average radius of relative stiffness of the test slabs, i.e., sufficient for load behavior to be similar to a slab of infinite surface area.

The equipment used to apply repetitive moving loads is shown in Figure 1. Load was applied through a 16-in. diameter wheel with a 4-in. wide solid rubber tire. The tire had longitudinal and transverse measurements scaled to represent the prototype. The contact area of the tire increased with increasing load as shown in Figure 3.

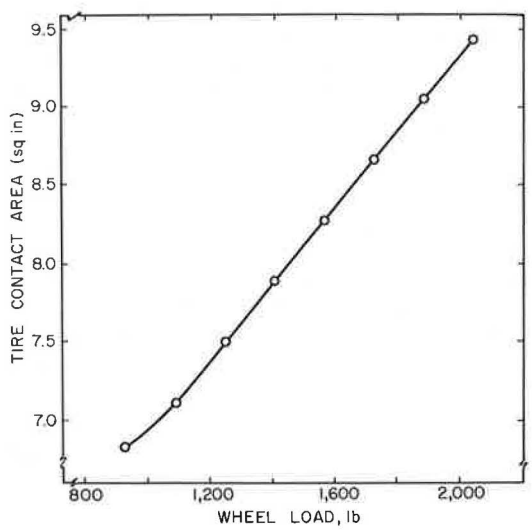

Figure 3. Contact area of solid rubber tire.

The paths traveled by the load wheel during the repetitive moving load tests are shown in Figure 4. Starting at location A, the wheel traveled 98 in. in a longitudinal path to location B. After returning in the same wheelpath to location A, the wheel was driven transversely a distance of 2 in. or half the width of the tire to a second longitudinal wheelpath. After returning to location C, the wheel was again driven transversely a distance of 2 in. to a third wheelpath. During each transverse movement of 2 in. the wheel traveled approximately 10 in. longitudinally. After traveling in 15 longitudinal wheelpaths or a total of 28 in. transversely to location D, the direction of transverse travel was reversed.

The Corps of Engineers (5) defines a load coverage as a sufficient number of vehicle operations or passes to produce

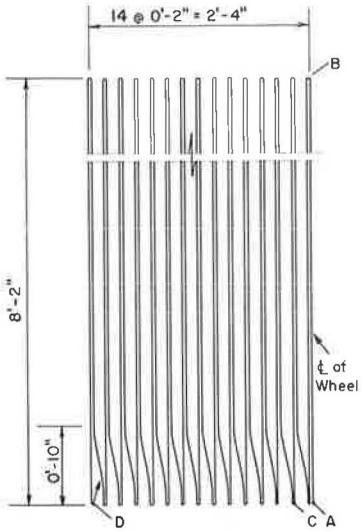

Figure 4. Wheelpaths during load testing.

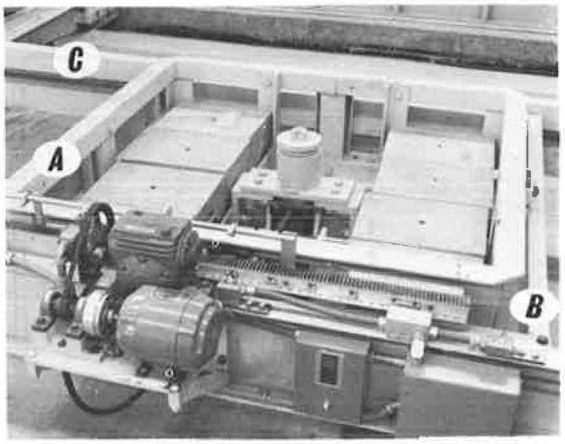

Figure 5. Load box.

statistically one application of the design loading over the entire traffic area. By this definition, 4 load coverages were applied each time the wheel traveled 28 in. transversely or from location A to D. The average wheel speed was 1.68 ft/sec and 106 coverages were applied per hour. Because this rate of loading is greater than that normally encountered on highway and airfield pavements, the data represent conditions more severe than those encountered in actual pavement service.

The load wheel was mounted in the center of a load box. To reduce transverse thrust on the test slabs when the wheel turned to change wheelpaths, the wheel was mounted as a caster with a swivel bearing. A spring mechanism was used to prevent the wheel from rotating 180 degrees on each return trip, as for example, from location B to A.

The load box, as represented by frame A in Figure 5, was made of steel angles welded together to form a frame 4 ft 5 in. by 4 ft 1 in. by 1 ft 5 in. deep. A pair of roller bearings that operated within a vertical channel at the center of each side of the load box enabled it to move freely in the vertical direction within frame B. The desired wheel load was obtained by placing concrete weights inside the load box.

Frame B was designed to move transversely within frame C by means of roller bearings that traveled on transverse bars bolted to the inside of the inside of the span beams of frame A. Power for driving frame B in the transverse direction was supplied by a ½-hp electric motor mounted on frame C. As shown in Figure 5, the motor acted through an electric clutch to drive a pinion gear over a rack mounted on frame B. Length of transverse travel was controlled by a number of stops contacting an electrical switch that regulated current to the clutch.

Frame C had a transverse span of 18 ft and a longitudinal length of 5 ft. A flanged crane wheel mounted near each corner traveled on longitudinal rails that were supported by steel beams independent of the subgrade and prestressing frame. Power for driving frame C in the longitudinal direction was supplied by a 5-hp electric motor. Operating through a gear reducer to obtain proper speed, the motor rotated a transverse steel shaft located near one end of the rails. Two steel drums were mounted on the shaft, one near each end between the flanges of the rail support beams. Each drum pulled a steel cable that traveled around a fixed pulley at the opposite end of the rails. Frame C was attached to the two cables to obtain longitudinal motion when the electric motor was operating. Length of longitudinal travel was controlled by an electrical switch that was activated when the load device passed either of two selected rail locations. This switch disconnected current and applied an electric brake to the motor. By regulating the electric current to the brake, the load device could be smoothly decelerated. An electrical switch on the motor shaft was used to determine when the load device had stopped and to start travel in the opposite longitudinal direction.

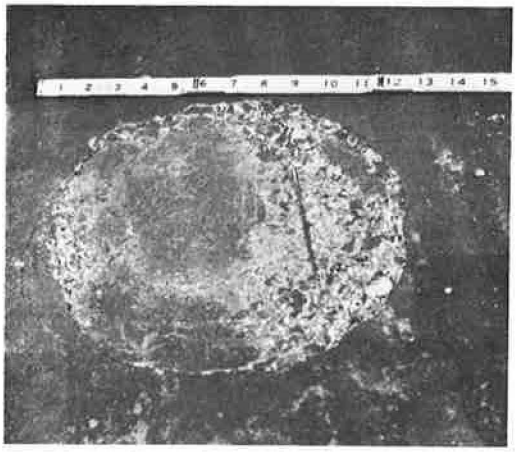

Figure 6. Failure in top surface of slab 2.

Instrumentation

Slab deflections were measured by a resistance bridge deflectometer (6) buried in the clay subgrade 2 ft below the test slabs. The deflectometer was restrained from vertical movement by a steel rod that extended between the deflectometer casing and the concrete slab under the clay subgrade. A second steel rod extended upward from the measurement control pin of the deflectometer to a fitting cast in the slab. An electrical connection between the deflectometer and chart recording equipment enabled deflections to be continuously measured as the load wheel approached and passed over the deflectometer location.

Strains were measured by pairs of SR-4 type A9-4 (2-in. long) strain gages cemented to the top surface of the test slabs, one in the longitudinal and one in the transverse direction at the same location. Strains were also recorded continuously as the load wheel approached and passed over the gages.

TEST RESULTS

Data are reported for load tests on 16 prestressed slabs. The spacing between prestressing wires, amount of tensile force in each wire, and resultant concrete prestress of each test slab are given in Table 4.

Moving loads were applied repeatedly to 15 of the test slabs until failure occurred. Wheel loads and number of coverages at failure are given in Table 5. Failure was characterized by a crumbling of the concrete in the top surface of the slab within a circular area approximately 12 in. in diameter (Fig. 6). These failures occurred very suddenly. Only a few additional load coverages were necessary for the top surface of the slab to deteriorate from the initial cracked condition to the failed condition shown. Failures occurred at random locations within the loaded areas. For most slabs, a thin steel plate was placed over the failed area and repetitive loading was continued until a second failure occurred. A bottom surface view of one of the slabs after a failure had occurred is shown in Figure 7. This photograph shows only a cut out interior portion of the slab where the moving loads were applied. Visual bottom surface cracks were indicated by black ink. Loose concrete was removed at the failure location to expose the prestressing wires. There were no wire failures during any of the load tests. After load testing

TABLE 4

REINFORCEMENT AND PRESTRESS PROPERTIES OF TEST SLABS

Slab No.	Wire Spacing (in.)		Wire Tensile Force (lb)	Concrete Prestress (psi)	
	Long.	Trans.		Long.	Trans.
1-8	12	12	1200	100	100
9	36	36	1200	33	33
10	None	None	0	0	0
11	12	12	140	12	12
12	12	0	1200	100	0
13-16	12	12	1200	100	100

TABLE 5

PROPERTIES OF TEST SLABS

Slab No.	Wheel Load (lb)	Coverages at Failure	h (in.)	k (pci)	L (in.)	a (in.)	α	m_c (in. lb./in.)
1	1730	5730	1.02	70	8.53	1.66	0.195	185
		7270	1.02	70	8.53	1.66	0.195	185
2	1571	2444	1.00	80	8.13	1.62	0.199	165
		3010	1.01	80	8.19	1.62	0.198	168
3	1571	2116	1.01	100	7.75	1.62	0.209	167
		2780	1.02	100	7.80	1.62	0.208	171
4	1410	2098	0.97	100	7.52	1.58	0.210	156
		3816	0.98	100	7.58	1.58	0.208	159
5	1410	25060	1.02	105	7.71	1.58	0.205	182
6	1730	330	0.96	110	7.28	1.66	0.228	155
		342	0.95	110	7.23	1.66	0.230	152
7	1571	472	0.92	120	6.90	1.62	0.235	140
		946	0.93	120	6.96	1.62	0.233	143
8	1571	6160	1.00	120	7.35	1.62	0.220	169
		7700	0.99	120	7.29	1.62	0.222	166
9	1571	7506	1.01	120	7.40	1.62	0.219	170
		8538	1.02	120	7.46	1.62	0.217	173
10	1571	860	1.01	120	7.40	1.62	0.219	163
11	1571	1676	1.02	120	7.46	1.62	0.217	170
12	1571	3226	1.00	120	7.35	1.62	0.220	159
13	Static Load Test		1.02	125	7.38	2.00	0.271	179
14	1730	18500	1.01	170	6.78	1.66	0.245	181
	Static Load Test		1.03	170	6.91	2.00	0.289	188
15	2049	1022	0.97	180	6.49	1.72	0.265	163
		1164	0.98	180	6.53	1.72	0.263	166
16	2206	0 to 14500[a]	1.00	320	5.75	1.76	0.306	171
	3478	14500 to 33700[a]	1.00	320	5.75	1.99	0.246	171

[a]Slab 16 did not fail.

was completed, slab thickness at each failed area was measured with a vernier caliper. Average thicknesses are given in Table 5.

A previous theoretical analysis (1) of prestressed concrete pavements indicated that strength is a function of α and m_c, where

$$\alpha = \frac{a}{L} \tag{1}$$

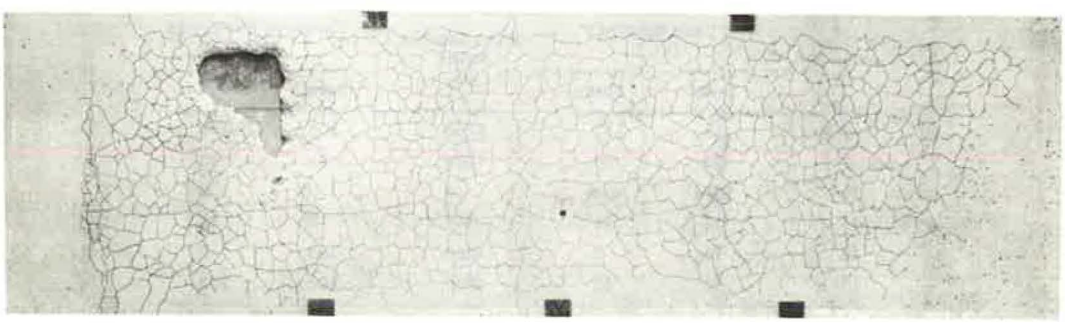

Figure 7. Crack pattern in bottom surface of slab 5.

and

$$m_c = \frac{\sigma_c h^2}{6} \tag{2}$$

in which

L = radius of relative stiffness (in.), i.e.,

$$L = \sqrt[4]{\frac{E h^3}{12 (1 - \mu^2) k}} \tag{3}$$

a = radius of loaded area (in.),
E = concrete elastic modulus (psi),
μ = Poisson's ratio,
h = slab thickness (in.),
k = subgrade modulus (pci),
σ_c = cracking stress (psi) = modulus of rupture plus prestress, and
m_c = cracking moment (in.lb/in. of width).

Computed m_c and α-values for each slab are given in Table 5. The radius of the loaded area, a, used to compute α-values was the radius of a circle having an area equal to that shown in Figure 3 for the loaded tire at the test load. The radius of relative stiffness, L, was computed using the measured value of 4,100,000 psi for the modulus of elasticity, E, and an assumed value of 0.15 for Poisson's ratio. The subgrade modulus, k, was determined with a 30-in. diameter plate at 0.05 in. deflection. The k-value given in Table 5 is the average of the values determined prior to the construction and after the testing of each slab. When computing m_c-values, cracking stresses were assumed to be equal to the summations of the modulus of rupture values given in Table 3 and the prestress values given in Table 4.

Analyses

To analyze the test data given in Table 5 and develop a design method for prestressed pavements, it is necessary to relate m_c and α-values with wheel loads and coverages causing failures. This may be done by using the m_c and α-values to compute either the bottom or the top surface cracking load of each slab, then establishing a relationship between the ratio of such cracking load to applied wheel load and the coverages causing failure.

Bottom Cracking

The following equation, based on Westergaard's (7) theoretical analysis for loads applied in the interior of the area of a panel, can be used to compute the bottom cracking load, P_c:

$$\left.\begin{matrix}\sigma_x \\ \sigma_y\end{matrix}\right\} = \frac{P}{h^2}\left[0.275\,(1+\mu)\log_{10}\frac{Eh^3}{k\left(\frac{a+b}{2}\right)^4} \mp 0.239\,(1-\mu)\,\frac{a-b}{a+b}\right] \tag{4}$$

where σ_x and σ_y = principal tensile stresses in the directions of x and y at the bottom of the slab under the center of the load, and a and b = semiaxes of an ellipse representing the footprint of a tire. For a circular loading area where a = b and letting $\mu = 0.15$, $L^4 = \frac{Eh^3}{12(1-\mu^2)k}$, $\alpha = \frac{a}{L}$, and $m_c = \frac{\sigma_x h^2}{6}$, Eq. 4 becomes:

$$P_c = \frac{m_c}{0.0527\left(4\log_{10}\frac{1}{\alpha} + 1.069\right)} \tag{5}$$

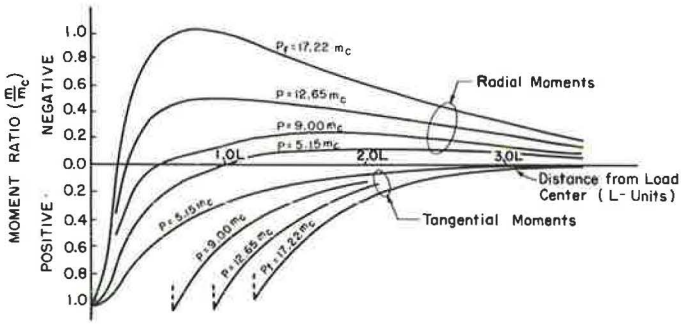

Figure 8. Radial and tangential moment curves—PCA theoretical method for $\alpha = 0.2$.

Top Cracking

The top surface cracking load of a prestressed pavement may be computed by the PCA theoretical method (1). This method is limited to a load applied at an interior position of a slab supported by a dense liquid foundation and prestressed equally in the longitudinal and transverse directions. By use of this method, radial and tangential moment diagrams were developed for loads greater than those causing bottom surface cracking, i.e., beyond conditions to which the elastic theory is applicable. Example moment diagrams for $\alpha = 0.2$ are shown in Figure 8. Bottom surface cracks begin to form under the load when the positive moment, m, equals the cracking moment, m_c, or when $m/m_c = 1$. A small increase in load beyond that initiating bottom cracking will cause these cracks to extend radially from the center of the load. As additional load is applied, there is an increase in the positive tangential moment and negative radial moment. The bottom surface radial cracks become longer, and the point of zero radial moment moves nearer the center of loading. At a load, P_F, equal to 17.22 times the cracking moment, m_c, the negative radial moment equals the cracking moment and a circular crack occurs in the top surface of the slab. Other top surface cracking loads predicted by the PCA method for α-values varying from 0.1 to 0.5 may be determined from the diagram shown in Figure 9.

Another method for computing top surface cracking loads is that used by the Corps of Engineers. Based on the results of previous static load tests on Hydrocal model slabs 16.6 in. square by 0.20 in. thick and supported on a 12-in. thick layer of natural rubber, the following empirical equation was developed (8):

$$P_F = \frac{h^2 (R + R_P)}{6\left[C\frac{M_o}{P_o} - \frac{M_R}{P_o}\right]} \qquad (6)$$

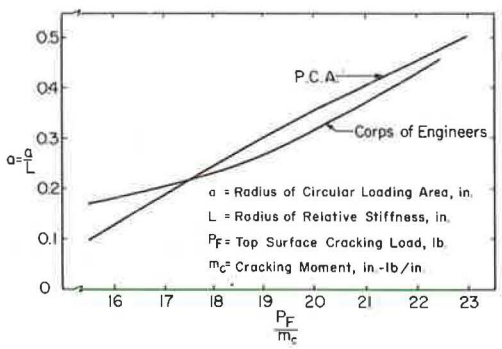

Figure 9. Top surface cracking loads for prestressed concrete pavements.

where

P_F = top surface cracking load (lb),
h = slab thickness (in.),
R = flexural strength of the concrete (psi),
R_P = concrete prestress (psi),
C = radial moment correction factor,
M_o/P_o = moment coefficient under center of loaded area, and
M_R/P_o = moment coefficient at point of negative moment cracking.

TABLE 6

DESIGN FACTORS BASED ON TOP CRACKING LOADS

Slab No.	Wheel Load (lb) P	Coverages at Failure	Bottom Cracking Load (lb) P_c	Top Cracking Load (lb) P_F			Fatigue Factors	
				PCA	C of E	Average	$\frac{P}{P_c}$	$\frac{P_F}{P}$
1	1730	5730	898	3170	3080	3125	1.93	1.81
		7270	898	3170	3080	3125	1.93	1.81
2	1571	2444	809	2800	2730	2765	1.94	1.76
		3010	824	2860	2790	2825	1.91	1.80
3	1571	2116	835	2900	2870	2885	1.88	1.84
		2780	855	2950	2910	2930	1.84	1.87
4	1410	2098	784	2730	2700	2715	1.80	1.93
		3816	795	2780	2740	2760	1.77	1.96
5	1410	25060	905	3150	3100	3125	1.56	2.22
6	1730	330	807	2720	2760	2740	2.14	1.58
		342	796	2680	2720	2700	2.17	1.56
7	1571	472	741	2500	2540	2520	2.12	1.60
		946	753	2540	2580	2560	2.09	1.63
8	1571	6160	867	2960	2960	2960	1.81	1.88
		7700	856	2920	2930	2925	1.84	1.86
9	1571	7506	870	2990	2990	2990	1.81	1.90
		8538	881	3060	3000	3030	1.78	1.93
10	1571	860	834	2920	2930	2925	1.88	1.86
11	1571	1676	866	2980	2980	2980	1.81	1.90
12	1571	3226	815	2940	2940	2940	1.93	1.87
13	Static Load Test		1017	3310	3420	3365	—	—
14	1730	18500	978	3260	3340	3300	1.77	1.91
	Static Load Test		1106	3530	3660	3595	—	—
15	2049	1022	916	2980	3080	3030	2.24	1.48
		1164	927	3040	3140	3090	2.21	1.51
16	2206	—[a]	1036	3270	3390	3330	2.13	1.51
	3478	—[a]	1118	3390	3510	3450	3.11	0.99

[a]Slab 16 did not fail.

In using this equation, values of C, M_O/P_O, and M_R/P_O must be obtained from appropriate curves (8). These values are plotted as functions of either A/L^2 or a/L where A is the area of the loaded area, a is the radius of the loaded area, and L is the radius of relative stiffness, so that it is possible to develop a relationship between P_F/m_c and a/L where m_c is equal to $h^2 (R + R_P)/6$. The resultant curve for circular loading areas is compared to the PCA method in Figure 9. It is seen that the two methods are in fair agreement.

Slabs on Clay Subgrade

Data are presented from tests on the nine slabs cast on a clay subgrade and prestressed to 100 psi in both longitudinal and transverse directions. Comparisons will later be made with the four slabs that had reduced amounts of prestress and with the three slabs cast on granular and cement-treated subbases.

Using the m_c and α-values given in Table 5, bottom surface cracking loads were computed by Westergaard's Eq. 5, and top surface cracking loads were computed by both the PCA and Corps of Engineers method using Figure 9. Top cracking loads by the two methods were nearly equal for each slab failure, and average values were used to determine ratios of computed top surface cracking loads divided by repetitive moving wheel loads. Also, ratios of repetitive moving loads divided by bottom surface cracking loads were determined. These ratios are given in Table 6 and in this report are defined as fatigue factors. Fatigue factors are plotted in Figure 10A and 10B vs the number of load coverages causing failure.

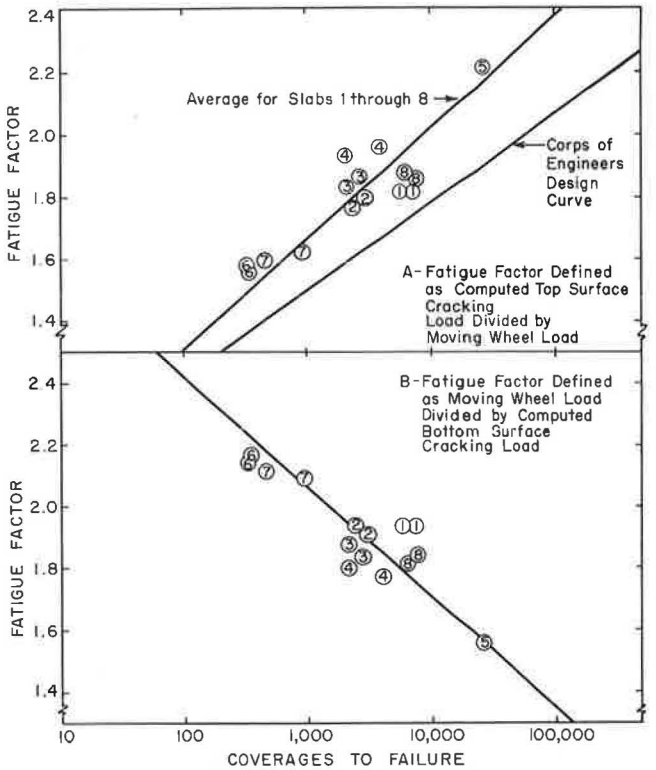

Figure 10. Fatigue relationships for prestressed concrete pavements.

The results of these tests may be compared with data from a similar moving load test program conducted by the Corps of Engineers (5). The essential differences between these two programs were as follows:

Characteristic	Corps of Engineers	PCA
Casting Technique	Precast	Cast in place
Prestressing: Method	Pretensioned	Pretensioned
Amount	250 psi	100 psi
Size of Slab: Length	15 ft	16 ft
Width	6 ft	12 ft
Thickness	1 in.	1 in.
Size of Loaded Area: Length	120 in.	98 in.
Width	24 in.	32 in.
Avg. Conc. Mod. of Rupt.	905 psi	914 psi
Avg. Conc. Elas. Mod.	4,500,000 psi	4,100,000 psi
Avg. Subgrade Modulus	65 pci	105 pci

In analyzing their data, the Corps of Engineers plotted a curve that related a design factor for repetitive loading to the number of load coverages causing failure. Their design factor was defined as the computed top surface cracking load for a single application divided by the repetitive moving wheel load. This curve is shown on the appropriate diagram in Figure 10A. For a given fatigue ratio, it indicates a greater number of coverages at failure than the PCA curve.

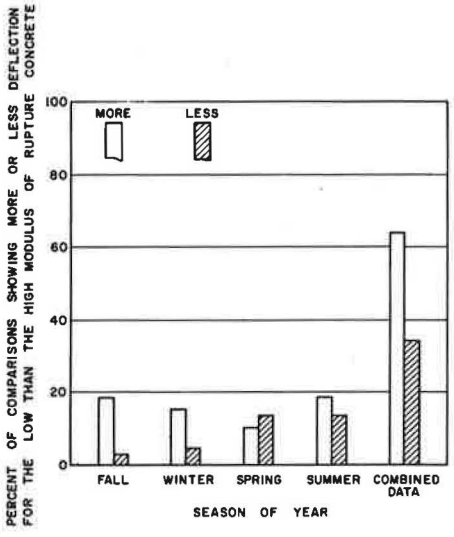

Figure 10. Deflection comparison of low and high modulus of rupture concrete.

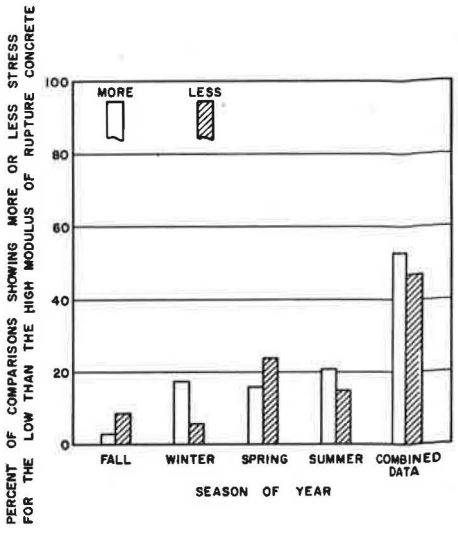

Figure 11. Stress comparison of low and high modulus of rupture concrete.

modulus deflected more than the high modulus of elasticity concrete. The range of modulus of elasticity experiencing the most deflection apparently varies slightly with season. Calculations have shown that, on the average, the lower modulus of elasticity concrete in general deflected 7.4 percent less than the high modulus of elasticity concrete. This finding, although contrary to rational reasoning, is in line with that found in another experiment (7).

Figure 9 is bar graph comparing modulus of elasticity against stress in the concrete slab. The graph structurally is the same as Figure 8 except that it portrays stress in the concrete. Inspection of Figure 9 shows that more comparisons of stress on low and high modulus of elasticity concrete showed less stress in the low than the high modulus concrete. The range of modulus of elasticity experiencing the most stress also varies with season.

The second concrete property considered here is the modulus of rupture. The analysis of the modulus of rupture was made by determining whether the deflections and stresses were more or less for the lower modulus of rupture concrete than the higher modulus of rupture CRCP. The evaluation was made for each season and also the combined data. Figure 10 shows in bar graph style the percentage of comparisons in which deflections on the high modulus of rupture concrete were more or less than those on the low modulus of rupture concrete. Note that the low modulus of rupture concrete deflects more than does the high. This was true for all seasons except for the spring. The combined data also show that the average deflection for all seasons is greater on the low modulus of rupture concrete.

The comparison of stresses on the low and high modulus of elasticity concrete indicate that, on the average, stresses were higher in the low than the high modulus of rupture concrete. Figure 11 shows the percent of comparisons in which the stress was higher or lower than that in the low modulus of rupture concrete.

Slab Thickness and Type—The pavement slab thickness analysis was made by comparing deflection measurements from sections that had identical classifications in the factorial, but different slab thickness. This allows a clean comparison of thickness to deflection and stress.

In each case the smaller thickness of concrete pavement was compared with a greater thickness. The results were combined for all four data runs. The comparison may not be very good because of the small number of sections compared.

TABLE 4

PERFORMANCE OF RIGID PAVEMENT IN TERMS OF THICKNESS, PAVEMENT TYPE, AND LOAD POSITION*

Thickness Comparison	Deflection		Stress	
	Crack or Joint	Midspan	Crack or Joint	Midspan
6-in. CRCP vs 8-in. CRCP	41.1	54.6	11.0	1.1
8-in. CRCP vs 9-in. JCP	-13.1	30.8	-50.2	-11.1
8-in. CRCP vs 10-in. JCP	-38.0	-28.5	-49.6	6.9

*Numbers indicate the average percent difference for the respective condition.

Table 4 is a summary of the results obtained in comparing pavements of different thickness and type. In comparing 6-in. CRCP with 8-in. CRCP, it was found that the 6-in. pavement deflected 41 percent more at the crack position than did the 8-in. CRCP. Comparing 8-in. CRCP with 9-in. JCP, it was found that the CRCP deflected on an average of 13.1 percent less than the JCP. When the 8-in. CRCP was compared to 10-in. JCP, it was found that the CRCP deflected on an average of 38 percent less than the 10-in. JCP.

It has been assumed in the past that 10-in. JCP performance would be very much the same as that of 8-in. CRCP (4). Performance measured in terms of deflection shows that the 8-in. CRCP is superior to the 10-in. JCP. In Figure 12 deflections as computed by the equations developed herein are plotted against deflections measured on comparable 10-in. JCP. The deflections for both pavement types have been corrected to zero temperature differential, and the deflections for CRCP were corrected to an 8-ft crack spacing and a 0.014-in. crack width. The data show a remarkable relation between the two parameters. By forcing the correlation line through zero (a rational approach), the slope of the line indicates that a 10-in. JCP deflects 1.6 times more than an 8-in. CRCP.

Deflection Position—On each test section a midspan deflection (between cracks) was obtained each time a reading was taken at the crack position. Figures 13 through 16 are plots of the average crack deflection versus the midspan deflection for each of the four runs. Although there is an offset on the vertical axis (crack deflection) greater than zero, it may be stated that the edge deflection and crack deflection are approximately equal on any range of support properties with continuous pavements that have 0.5 percent longitudinal steel or greater.

The radius of curvature measurements were also plotted in the same manner as deflection measurements (Figs. 17 through 20). In the case of radius of curvature—in contrast to deflection—the crack position has considerably less magnitude than the midspan position, which means that the concrete at the crack position is experiencing considerably more stress.

In terms of deflection and radius of curvature, it is evident that the aggregate interlock produces adequate load transfer across a crack, but the transverse cracks affect the continuity condition of the slab.

Semi-Controlled Variables

Two factors studied on a semi-controlled basis were the season of the year that the field measurements were taken and the general moisture condition of the soil.

Season—Data were taken on a statewide basis in each of the four seasons of the year. The deflection and radius of curvature data taken during these four seasons were analyzed by comparing each set of data with that taken during the summer. The comparison showed only whether the deflections and stresses were more or less in the fall, winter, and spring than in the summer. In Figure 21 these comparisons showing more or less deflection than the summer data are expressed as percentages. The results indicate that the deflections during fall and winter were generally greater than the summer, whereas the spring deflections were significantly smaller than the summer. Thus the

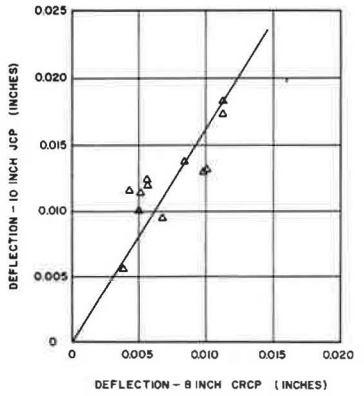

Figure 12. Calculated 8-in. CRCP deflection vs measured 10-in. JCP deflection.

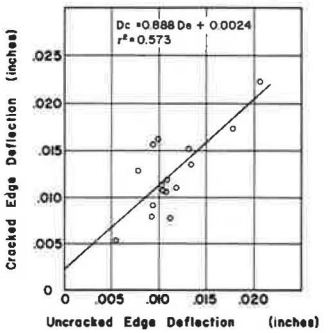

Figure 13. Cracked edge vs uncracked edge deflection—fall.

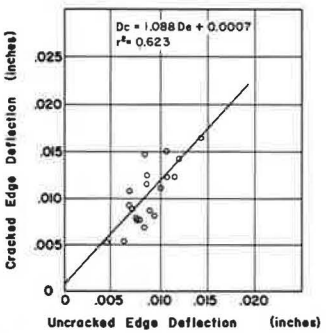

Figure 14. Cracked edge vs uncracked edge deflection—winter.

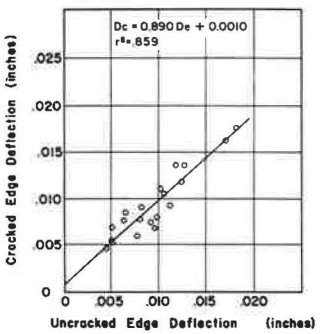

Figure 15. Cracked edge vs uncracked edge deflection—summer.

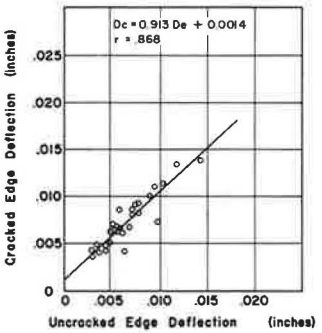

Figure 16. Cracked edge vs uncracked edge deflection—spring.

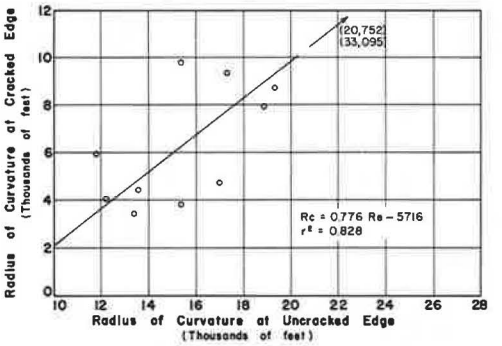

Figure 17. Cracked edge vs uncracked edge radius of curvature—fall.

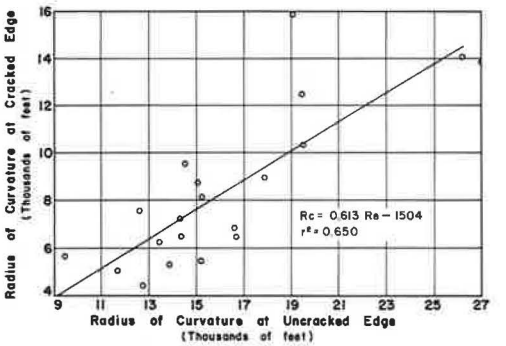

Figure 18. Cracked edge vs uncracked edge radius of curvature—winter.

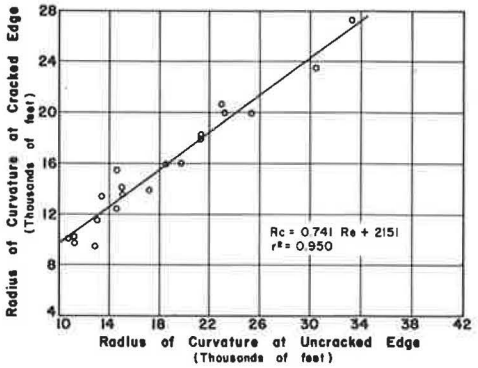

Figure 19. Cracked edge vs uncracked edge radius of curvature—summer.

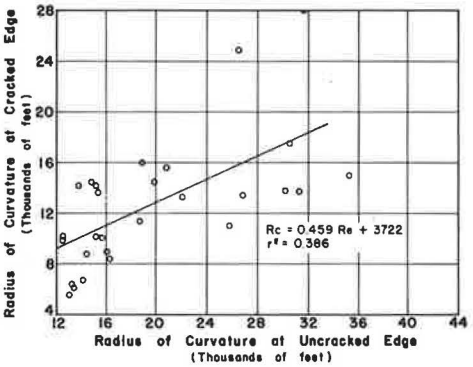

Figure 20. Cracked edge vs uncracked edge radius of curvature—spring.

deflection might in some way be related to the season; however, for the fall and winter there was not very much difference in the data.

The results of the stress analysis shown in Figure 22 indicate that the seasonal comparisons with the summer data are consistent in showing that the pavements experience less stress in the summer than during the other seasons.

Soil Moisture Condition—Each time data were taken on a test section, the general environmental conditions of the soil adjacent to the roadway in a hole 1 ft deep was classified as dry, moist, or wet. As far as the moisture effects are concerned, it was found that the fourth data run, which was the spring run, measured deflections that were much less. During the entire spring run general rains were experienced over the state. Of the four runs, the spring run was by far the wettest.

CORRELATION OF VARIABLES

Deflection

The variables studied that affect deflection are the crack spacing, surface crack width, concrete modulus of elasticity and modulus of rupture, pavement slab thickness, pavement type, strength characteristics of the subgrade and subbase, and moisture conditions. With the exception of the semi-controlled variables and the modulus of rupture, these variables will be correlated into an equation in the following.

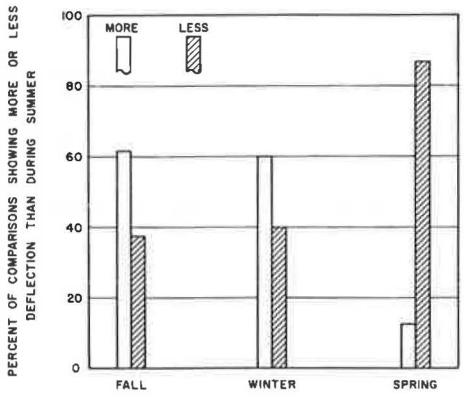

Figure 21. Seasonal comparison of deflection.

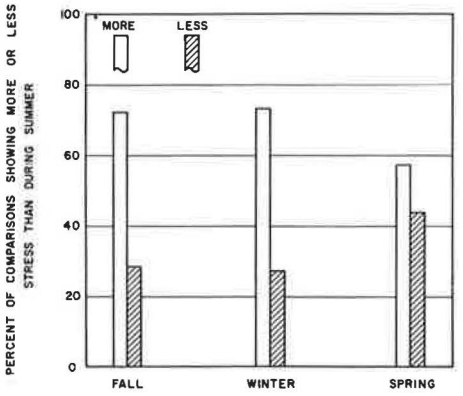

Figure 22. Seasonal comparison of stress.

A model equation was developed which encompassed the variables to be correlated. The model was based on previous work and also on work done at the AASHO Road Test (5, 8). The model chosen to relate the variables is basically an extension of the Road Test model and is of the following form:

$$D_c = \frac{A_0 \, L \, 10^{B_5 \, \Delta X} \, \overline{X}^{B_4}}{D^{1.75} \, E^{B_2} \, SS^{B_3} \, 10^{0.0147 \, T}} \tag{1}$$

where

L = Load in kips;
X = Surface crack width in inches;
$\overline{X}$ = Average crack spacing in feet;
D = Slab thickness in inches;
E = Concrete modulus of elasticity, psi;
SS = Soil support;
D_c = Deflection at crack position, inches;
D_e = Deflection at midspan position, inches;
T = Temperature differential between top and bottom of the slab, degrees F; and
A_0, B_1, B_2, B_3, B_4, and B_5 are constants determined from a regression analysis on the data.

Slab thickness was not truly a full factorial variable, and consequently could not be entered as an independent variable and had to be analyzed separately. All the subsequent regression analyses were performed for the 8-in. pavement thickness factorial. The 1.75 power for the thickness term will be established later.

The soil support term is a combination of the subgrade and subbase strength characteristics. The soil support is a calculated value developed in a previous analysis. In some cases the natural soil was stabilized with lime (generally clay) to facilitate construction operations by providing a working platform.

The soil support is defined as

$$SS = \left(\frac{U_1 + U_2}{T_{sg}}\right) \tag{2}$$

where

SS = Soil support;
U = Unconfined compressive strength of subbase and subgrade materials in psi at an age of 7 days;
T_{sg} = Texas triaxial classification of subgrade material; and
1, 2 = Subscripts denoting subbase and stabilized subgrade respectively.

In all subsequent analysis the load, L, will be 18 kips and the pavement slab thickness will be 8 in. The linear form of load used here has been qualified in another report on this project (7) and in studies by others (5). The data from each run were carefully analyzed to screen out what might be considered erroneous.

The power term for the temperature differential term was derived in another report on this overall study (8). The temperature differential, the pavement thickness, and the load terms were not a part of the full factorial experiment, but in order that their effect would be reflected in the A_0 term, constant values for the 8-in. factorial were inserted into the equation for variables not considered in the semi-factorial experiment. The values inserted into the equation were an 18-kip single axle load, 8 in. for pavement thickness, and zero for temperature differential. These factors were then considered as constant and moved to the left of the equation.

A multiple regression analysis was made using the computer on each data run for deflection at the crack position, D_c, and also for deflection midway between cracks, D_e. The constants and the statistics derived from the regression analysis of each of the four runs are given in Table 5.

TABLE 5

COMPUTED CONSTANTS AND STATISTICS FROM REGRESSION ANALYSIS*

Load Position	Data Run No.	Computed Values							
		A_0	B_2	B_3	B_4	B_5	r	r^2	σ
Crack	1	6.664	0.334	0.681	-0.060	3.222	0.698	0.487	±0.0032
	2	0.00256	-0.123	0.526	0.1100	13.437	0.551	0.303	±0.0029
	3	0.1220	0.104	0.690	0.0900	13.911	0.662	0.438	±0.0030
	4	0.1099	0.1249	0.6869	0.0794	13.575	0.694	0.482	±0.0021
Midspan	1	0.0118	-0.0684	0.3211	-0.1938	7.816	0.407	0.166	±0.0035
	2	0.0726	0.0418	0.3434	-0.3294	7.055	0.244	0.060	±0.0032
	3	0.00373	-0.124	0.8709	0.1814	11.798	0.733	0.538	±0.0027
	4	0.0749	0.1026	0.7179	0.1897	4.876	0.515	0.265	±0.0031

*FOR EQUATION 1: r = coefficient of correlation, r^2 = coefficient of determination, σ = standard error of estimate.

The calculated deflection was plotted against the measured deflection for each data run and for each load position. These graphs are shown in Figures 23 through 30. Note the same general pattern for runs 1, 2, and 3 for both the crack and midspan deflections. The deflections at both crack and midspan were very small on run 4, as discussed previously, when compared with the three previous data runs.

In Table 5 note that several values of B_4 are negative. This same result was the case in a previous analysis (8). The crack spacing deflection relationship is a bowl-shaped curve, concave upwards. When the crack spacing is greater than that at the point of zero slope, B_4 is positive, and when it is smaller, B_4 is negative. Figure 31 is an example of the deflection-crack spacing relationship that results in a change of signs on B_4.

Several of the values calculated for B_2 are also negative. B_2 is the exponent on the modulus of elasticity term in the model equation. A negative B_2 would be in disagreement with theoretical concepts. Earlier it was pointed out that the low modulus of elasticity CRCP was deflecting less than the high modulus of elasticity CRCP. Another investigation on an experimental CRCP showed this same factor between lightweight and conventional aggregate concrete (7).

Note that the constants for each variable term generally have approximately the same magnitude, with only a few exceptions. The data from the first three runs were comparable, and therefore they were combined and a regression analysis was run. This resulted in two final equations, one for deflection at the crack position and another for deflection at a point midway between cracks. The computed constants and statistics are given in Table 6. The equation would be applicable to a dry condition; for a wet condition the equation for run 4 would be used. Note that the standard error is only slightly greater than the resolution of the Benkelman beam.

Radius of Curvature

The radius of curvature data have been examined thus far in terms of stress, but the subsequent analysis will be in terms of the radius of curvature data.

TABLE 6

COMPUTED CONSTANTS AND STATISTICS FOR DEFLECTION EQUATIONS

Load Position	Regression Analysis Computations							
	A_0	B_2	B_3	B_4	B_5	r	r^2	σ
Crack	0.3779	0.1683	0.6513	0.0266	6.3407	0.6971	0.486	±0.0028
Midspan	0.1362	0.0977	0.5601	-0.0462	4.1266	0.5544	0.307	±0.0033

Note: r = coefficient of correlation, r^2 = coefficient of determination, σ = standard error of estimate.

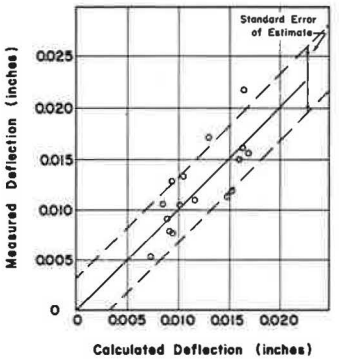

Figure 23. Measured vs calculated deflection at cracked edge—fall.

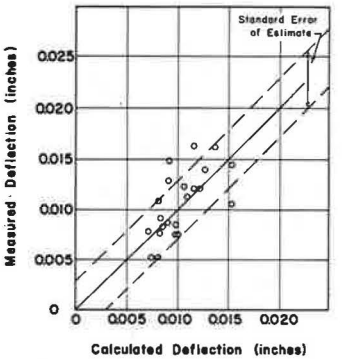

Figure 24. Measured vs calculated deflection at cracked edge—winter.

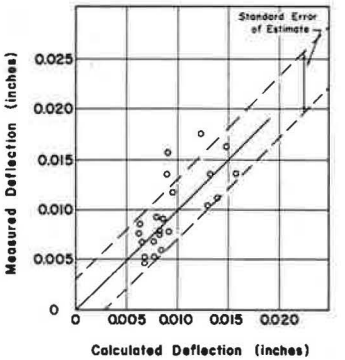

Figure 25. Measured vs calculated deflection at cracked edge—summer.

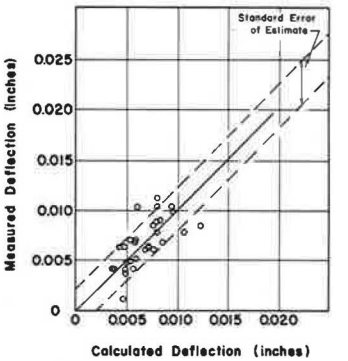

Figure 26. Measured vs calculated deflection at cracked edge—spring.

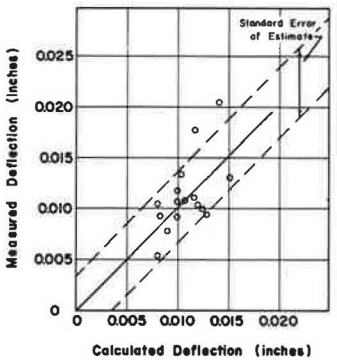

Figure 27. Measured vs calculated deflection at uncracked edge—fall.

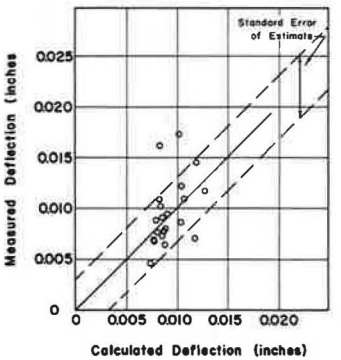

Figure 28. Measured vs calculated deflection at uncracked edge—winter.

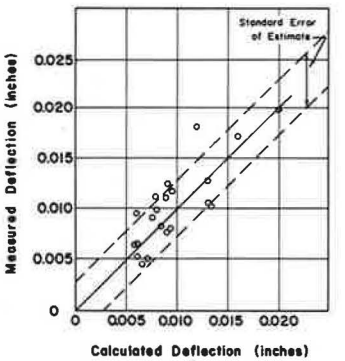

Figure 29. Measured vs calculated deflection at uncracked edge—summer.

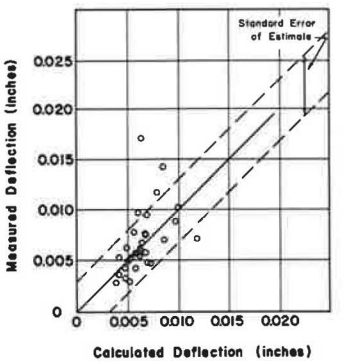

Figure 30. Measured vs calculated deflection at uncracked edge—spring.

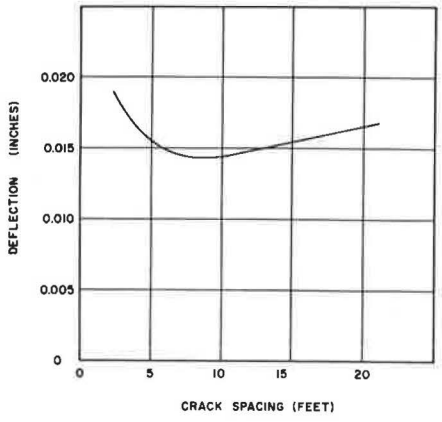

Figure 31. Deflection vs crack spacing.

The variables investigated that might affect the radius of curvature are the average crack spacing, soil support, concrete modulus of elasticity, load, and slab thickness. Thus, radius of curvature is some function of all these variables:

$$R_c,\ R_e = f(\overline{X},\ SS,\ E,\ L,\ D)$$

where

R_c = Radius of curvature at crack position, and

R_e = Radius of curvature at midspan position.

All other terms have been defined previously.

A model equation for radius of curvature was logically derived using the same concept as developed in the deflection equation. The following is the model with variables considered:

$$R_c = \frac{A_0\, D^{1.75}\, E^{B_2}\, SS^{B_3}\, \overline{X}^{B_4}}{L} \qquad (3)$$

All terms are as previously defined.

In the radius of curvature study the slab thickness again could not be entered as an independent variable because of a shortage of test sections on pavement thinner than 8 in. Thus the same thickness term was used here as in the deflection analysis, $D^{1.75}$.

Although the crack width and temperature differential are not reflected in Eq. 3, they were considered in this study and previous studies. Previous studies indicated that the effect of temperature differential on the radius of curvature was very slight or nonexistent. Therefore, on this basis, the temperature differential term was deleted. With regard to crack width, this term was included in the equation, but it was found that the statistics of correlation were improved by deleting it from the regression equation.

The radius of curvature of the CRCP is studied at two points on the continuous slab, across the volume change crack and midway between the cracks. The crack radius of curvature was analyzed for each data run except the fourth. The individual data runs were analyzed using multiple regression techniques. The regression constants for the model equation are given in Table 7. In order to obtain a more general equation for the radius of curvature at the crack position, the field data were examined and runs 1 and 2 were combined to form the data for the regression that would produce the final equation for radius of curvature at the crack position. Figures 32 through 35 show the measured radius of curvature plotted against the calculated radius of curvature for the crack position for runs 1, 2, and 3 and the combined data. The computed constants and the statistics for the final equation are given in Table 8.

TABLE 7

COMPUTED CONSTANTS AND STATISTICS FROM RADIUS OF CURVATURE ANALYSIS*

Load Position	Data Run No.	Computed Values						
		A_0	B_2	B_3	B_4	r	r^2	σ
Crack	1	0.000832	0.9819	0.6572	-0.2623	0.9518	0.9059	± 962
	2	350.5333	0.1548	0.3429	-0.1766	0.5574	0.3107	±1716
	3	53.4066	0.2898	0.4070	-0.0035	0.6900	0.4762	±2132
Midspan	1	0.0742	0.7395	0.1882	0.0277	0.9527	0.9076	± 868
	2	1779.2667	0.0639	0.3102	0.0863	0.4368	0.1908	±2247
	3	313.4298	0.1736	0.5872	0.0345	0.7503	0.5630	±2798
	4	1337.6603	0.0832	0.2894	0.1147	0.4453	0.1983	±2525

*FOR EQUATION 3: r = coefficient of correlation, r^2 = coefficient of determination, σ = standard error of estimate.

TABLE 8

COMPUTED CONSTANTS AND STATISTICS FOR RADIUS OF CURVATURE EQUATIONS

Load Position	Regression Analysis Computations						
	A_0	B_2	B_3	B_4	r	r^2	σ
Crack	15.3039	0.3312	0.5467	-0.0772	0.6391	0.4085	±1617
Midspan	333.3153	0.1729	0.3579	0.0909	0.5957	0.3548	±2508

Note: r = coefficient of correlation, r^2 = coefficient of determination, σ = standard error of estimate.

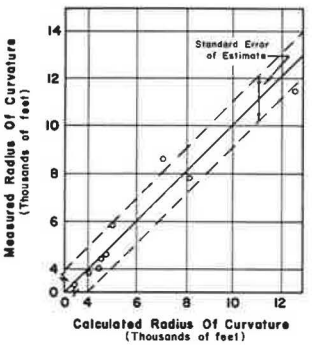

Figure 32. Measured vs calculated radius of curvature at cracked edge—fall.

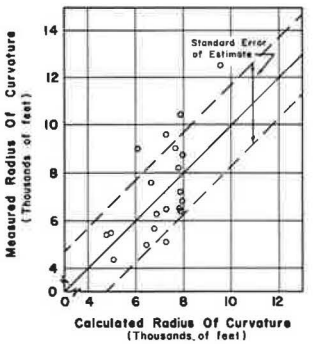

Figure 33. Measured vs calculated radius of curvature at cracked edge—winter.

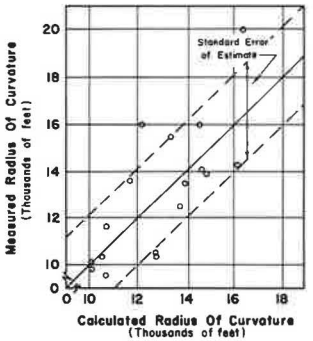

Figure 34. Measured vs calculated radius of curvature at cracked edge—summer.

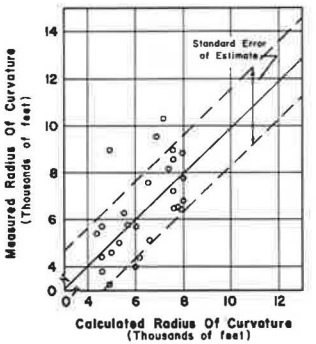

Figure 35. Measured vs calculated radius of curvature—combined data.

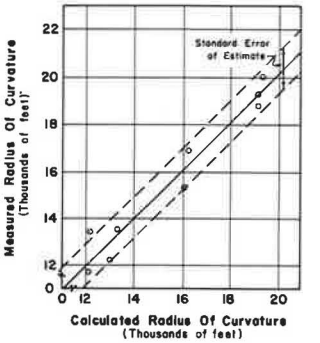

Figure 36. Measured vs calculated radius of curvature at uncracked edge—fall.

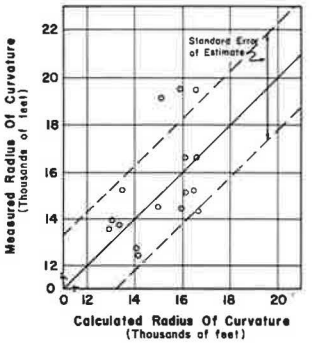

Figure 37. Measured vs calculated radius of curvature at uncracked edge—winter.

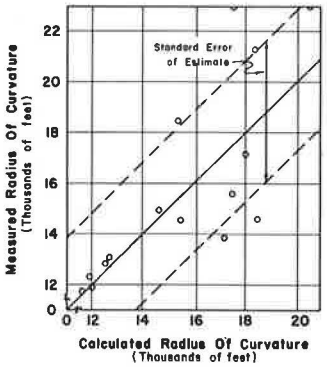

Figure 38. Measured vs calculated radius of curvature at uncracked edge—summer.

The midspan radius of curvature data were analyzed in like manner as the crack radius data; however, here all four data runs were used to relate the parameters studied to radius of curvature. The computed constants and statistics for the four equations are given in Table 8. Figures 36 through 39 show the calculated radius of curvature plotted against the measured midspan radius of curvature.

DISCUSSION OF RESULTS

Deflection

In general, the control variables considered in this study were found to affect the deflection of a CRCP. Their effect follows a pattern that can be expressed by a mathematical expression. Of the semi-controlled variables considered, it was found that the soil moisture condition affected the deflection, although the findings were contrary to the generally accepted criteria of greater deflection for a moist condition. In addition, the findings of this study tend to verify the assumptions used in the design and development of CRCP.

Soil Moisture—The four data runs were made in different seasons over a period of about two years. At the times the data were taken, the general soil moisture conditions were not the same. The fourth run was exceptionally wet, and deflections on this run were all considerably less than they had been on the first three runs. Initially, this discrepancy between the findings and the normal assumption of more deflection for a wet condition caused much concern for errors that might have been made on the fourth run in taking the data. When the weather conditions were the same as on the fourth run, the pavement deflections on approximately one-third of the sections were measured again. As was the case previously, the deflections were small and for all practical purposes identical to those of the fourth run.

It is now believed that when the subgrade and subbase materials are saturated they respond to quick loading as does a soil sample in an undrained triaxial test. The load applied to the pavement is supported partially by the pore water in the pavement foundation rather than the soil grains as is the case where the soil is not saturated (13).

It should also be pointed out that the summer run, where the soil was the dryest, experienced slightly less deflection than periods when the subsoil was partially saturated. Of course, this latter condition could be the result of smaller cracks due to summer temperatures.

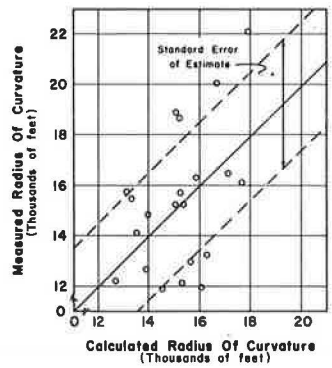

Figure 39. Measured vs calculated radius of curvature at uncracked edge—spring.

Equations—The deflection equations derived herein are extensions of the one developed in an earlier report (8). The previous equation was based on data taken from only two test sections, and those herein are based on 20 pavements with three sets of data from each for the dry condition and one set for the wet run. Table 9 gives a comparison of the equations with the equation developed earlier (8), which was based on crack position data only.

Figures 40 and 41 were prepared to illustrate the capability of the equation for predicting the observed deflection. In each case, the regression equation developed from the data for both the crack position and midspan position was used to calculate the deflection for a given set of conditions on a test section. This calculated deflection was then compared against measured deflections for the test sections as portrayed in the figures. Note the close

agreement, in most cases, between the measured and calculated values. In some cases, both the measured and calculated deflection appear to be out of line with what is to be expected, but these exceptions are normally due to a lime-stabilized subgrade and are so marked on the figures. These figures are typical of all runs, and hence, these observations support the validity of using these equations in design work.

TABLE 9

COMPARISON OF REGRESSION ANALYSIS CONSTANTS

Constant	Overnight Study	Statewide Study
A_0	0.0106	0.3779
B_2	—	0.1683
B_3	0.8503	0.6513
B_4	0.0994	0.0266
B_5	4.8997	6.3407

$$D_C = \frac{A_0 L 10^{B_5 \Delta X} \bar{X}^{B_4} T_{sg}^{0.25 B_3}}{D^{1.75} E^{B_2} U^{0.25 B_3} 10^{0.0147 T}}$$

Modulus of Elasticity—The findings in this study in regard to the modulus of elasticity of concrete contradict the generally accepted theory of a lower modulus of elasticity slab deflecting more than a high modulus one for equal conditions. Although the levels of the modulus are not too far apart in magnitude, another experiment on this same research project, wherein the levels were considerably greater through the use of two entirely different coarse aggregate types, indicated the same results. These two separate investigations, along with a limited laboratory investigation,

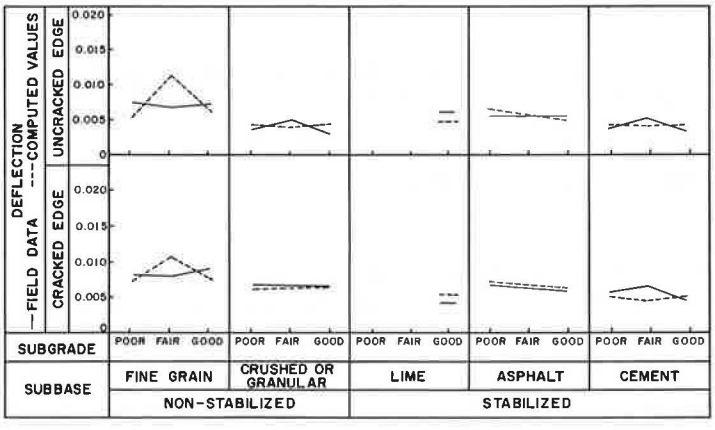

Figure 40. Measured and computed deflections on high modulus of elasticity concrete.

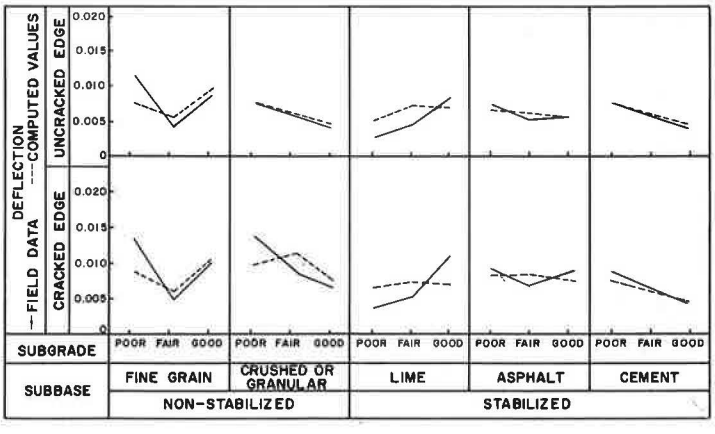

Figure 41. Measured and computed deflections on low modulus of elasticity concrete.

lend credence to the observations of less deflection with a lower modulus of elasticity concrete (14). It should be emphasized, however, that this observation can only be related to CRCP at this time and should not be translated to JCP, which may react differently.

There is a good possibility that this controversial observation attributed to modulus of elasticity could be an indirect effect of a combination of variables not considered in this experiment.

It may be hypothesized that generally speaking, a low modulus of elasticity concrete has a lower coefficient of thermal expansion. In this case the transverse volume change cracks would be smaller, and hence a greater degree of load transfer would be available. Therefore, with a greater load transfer less deflection would be experienced.

Furthermore, in the normal theoretical analyses of this condition, such as those of Westergaard, Pickett, Spangler, etc., the basic assumption is made that the subgrade reaction forces are vertical. An actual pavement on a subgrade deflecting under a wheel load develops a complicated interaction of shear forces and vertical forces, which may result in these field observations rather than those developed in a simplified theoretical approach.

Final Equation—The equations developed contain the term soil support, which was defined by Eq. 2. The soil support term can be eliminated from the deflection equations by substitution of Eq. 2 into Eq. 1. The dry or partially saturated condition was used as the level for selecting the final equation. Thus, the equation for deflection takes the form

$$D_C = \frac{0.3779\ L\ 10^{6.3407\ \Delta X\ \bar{X}^{0.0266}\ T_{Sg}^{0.1628}}}{D^{1.75}\ E^{0.1683}\ (U_1 + U_2)^{0.1628}\ 10^{0.0147\ T}}$$

where all terms are as previously defined.

Radius of Curvature

The radius of curvature data show that the average radius of curvature at the cracked edge for all data is about 52 percent less than the radius of curvature at the uncracked edge. The radius of curvature at the crack and midspan was correlated by linear regression analysis for each of the four data runs, and the graphs were shown in Figures 17 through 20.

Figures 42 and 43 show calculated and measured radius of curvatures plotted against the subgrade classifications for each subbase material type that was available.

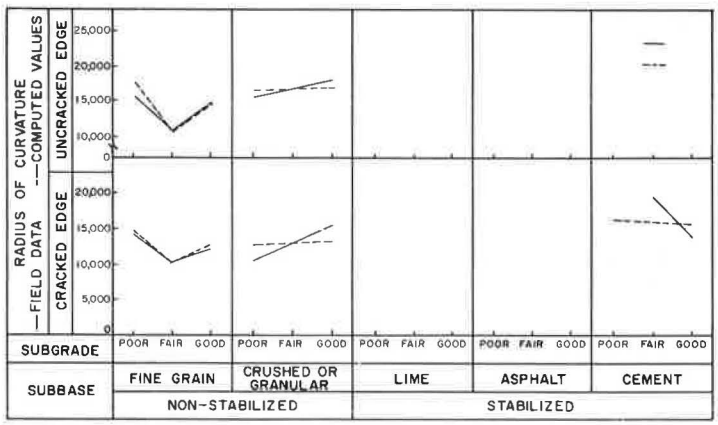

Figure 42. Measured and computed radius of curvatures on high modulus of elasticity concrete.

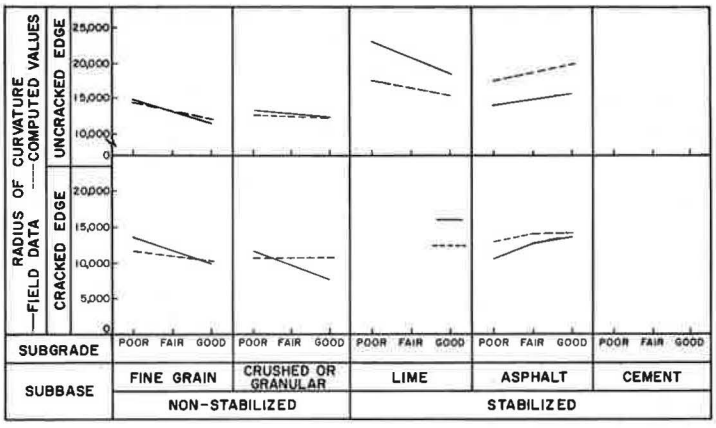

Figure 43. Measured and computed radius of curvatures on low modulus of elasticity concrete.

Final Equation—The radius of curvature equations determined for combined data contained the soil support term. Here again, the definition of soil support can be substituted and the radius of curvature equation will then take the form

$$R_c = \frac{15.3039\ D^{1.75}\ E^{0.3312}\ (U_1 + U_2)^{0.1367}}{L\ T_{sg}^{0.1367}\ \bar{X}^{0.0772}}$$

where all terms are as previously described.

An attempt was made to add the crack width as another variable but the results were such that it would be better not to include the crack width.

Accuracy of Regression Equations

Nineteen sets of deflection and radius of curvature data were analyzed by multiple regression methods. For each analysis a value of r, the correlation coefficient, was obtained. These values of r were checked against a table for their significance for the number of points and degrees of freedom (15). Table 10 gives the results of the r check.

The regression results appear to substantiate the form of the model equations. All checks on the correlation coefficients from the analysis of combined data were above that required to be significant. Previous discussions showed that the standard error of these equations is compatible with the accuracy of the equipment used. Thus the equations are in most cases statistically sound.

TABLE 10

INVESTIGATING THE SIGNIFICANCE OF CORRELATION COEFFICIENTS

Analysis	Crack	Midspan
Deflection:		
Run No. 1	G	F
Run No. 2	G	F
Run No. 3	G	G
Run No. 4	G	G
Combined data	G	G
Radius of Curvature:		
Run No. 1	G	G
Run No. 2	G	F
Run No. 3	G	G
Run No. 4		F
Combined data	G	G

G—The coefficient of correlation is greater than a minimum value required for significance.
F—The coefficient of correlation is less than a minimum value required for significance.

Validation of Design Assumptions

The findings of this study provide validity for the assumptions used in the original design analysis of CRCP. The equal magnitude of deflection at the crack position and midspan position indicates that sufficient granular interlock is provided so that approximately 100 percent load transfer is experienced across a crack. This finding is applicable only where the pavements have 0.5 percent longitudinal steel or more,

although there is a possibility that the lower limit on percent steel may be less than the minimum used in this experiment. Considering these aspects, this finding is applicable over a wide range of support conditions and concrete properties and components.

Furthermore, the use of the Westergaard interior loading conditions for determining the pavement thickness is a satisfactory procedure. The findings of this experiment indicate a 2-in. differential between CRCP and JCP and are in agreement with field performance from a deflection standpoint. This finding also has validity over a wide range of support conditions and concrete properties.

Design Equations

The final equations presented here for both deflection and radius of curvature provide excellent criteria for developing equations to be used in the design of concrete pavements. Although there are numerous factors other than deflection and stress to consider in the design of concrete pavements, this material will present another guideline for a designer to use in selecting the final pavement structure design for a given roadway.

Although percent longitudinal steel and pavement type are not enumerated in these design equations, they may be inserted on the basis of other material and studies developed in connection with this project. These are empirical equations and care should be taken not to extrapolate beyond the limits used in this analysis. The following are some suggested boundary conditions for extrapolation:

D_C = 0.003 in. to 0.030 in.
E = 3×10^6 psi to 6×10^6 psi
D = 6 to 8 in. for CRCP
D = 8 to 10 in. for JCP
$\overline{X}$ = 3 to 12 ft

CONCLUSIONS

This deflection study of CRCP has encompassed a wide variety of conditions and a considerable part of the geographical area of the state. The study was conducted over a 3-year period and over 15,000 separate measurements of various types were used. As a result of this field study and analysis, the following conclusions are warranted:

1. The variables studied herein that were found to affect the deflection of CRCP were concrete modulus of elasticity, modulus of rupture, crack spacing, surface crack width, pavement slab thickness, pavement type, strength characteristics of the subgrade and subbase, and subsurface moisture conditions. An empirical equation was derived using these variables, except modulus of rupture and moisture condition, to predict the deflection of a continuously reinforced concrete pavement under a given wheel load.
2. An equation was also derived from the study that predicts the radius of curvature of a pavement, i.e., related to pavement stress, in terms of the same variables with the exception of crack width.
3. It is recommended that the final equations derived herein be used to develop a nomograph predicting the deflection and radius of curvature for the variables studied. Through the use of this nomograph along with a maximum allowable deflection, pavements may be designed and/or checked in terms of the conditions existing on each project.
4. For the design equation mentioned, the variables of pavement type and percent longitudinal steel may be added to the equation on the basis of the studies herein and previous studies made in connection with this research project.
5. For continuous pavements, longitudinally reinforced with 0.5 percent steel or greater, it was found under a wide variation of support and environmental conditions that the transverse cracks in CRCP are small enough to retain sufficient aggregate interlock to maintain approximately 100 percent load transfer across the crack.
6. The transverse cracks were found to affect the continuity of a CRCP, since measurements indicated that the radius of curvature was smaller, i.e., there was greater stress at the crack than at a midspan point between cracks.
7. From a deflection and stress standpoint, pavements with stabilized subbases are superior in performance to pavements with non-stabilized subbases. All three of the

stabilizing agents considered in this study were found to give excellent performance from a deflection standpoint, but as a result of other studies that will be presented in the future, it is recommended that lime-stabilized subbases be protected with a non-erosive material.

8. From a deflection standpoint, the present practice of using a 2-in. thinner pavement for CRCP in relation to JCP as indicated by current design procedures is correct and conservative. For a given set of conditions, it was found that the deflection for an 8-in. CRCP is equal to or less than for a 10-in. JCP.

9. This study indicated that a reduction in thickness for CRCP had slightly more effect on deflection than an equal reduction in thickness for jointed pavement as found at the AASHO Road Test. Although there is a slight variation, the effect of pavement thickness on deflection as found by (a) this study, (b) the AASHO Road Test, and (c) Westergaard's theoretical analysis are in approximately the same range.

10. The use of a lime-stabilized subgrade, as practiced in Texas, for a working platform or moisture control was found to give an additional benefit of substantially reducing the deflections of a continuous pavement. Under certain conditions, the supporting characteristics of this layer may be considered in design.

11. From a deflection and stress standpoint, the design details presently being used by the Texas Highway Department for CRCP appear to be more than adequate for the conditions found in Texas.

12. This study developed two findings that contradict widely accepted beliefs concerning deflection of concrete pavement: (a) It was found that pavement on moist or saturated foundations deflected less than when the support was dry or partially saturated; These observations were confirmed during two different wet periods and three dry periods. (b) Although the difference is small, deflections and stresses are lower on low modulus CRCP than on high modulus concrete.

ACKNOWLEDGMENTS

The research reported herein was conducted under the supervision of Robert L. Lewis, Research Engineer, and under the general supervision of T. S. Huff, Chief Engineer of Highway Design, Texas Highway Department. The authors wish to extend their thanks to H. D. Swilley, Senior Laboratory Engineer, District 2; B. R. Hunter, Supervising Laboratory Engineer, District 3; Robert L. McKinney, Geologist, District 9; Billy Rudd, Senior Laboratory Engineer, District 10; Franklin J. Shenkir, Senior Laboratory Engineer, District 12; Clarence A. Weise, Supervising Resident Engineer, District 13; Charles W. Baxter, Senior Laboratory Engineer, District 15; Jerry Nemec, Supervising Resident Engineer, District 17; Wilburne C. Gromatsky, Supervising Construction Engineer, District 18; John W. Livingston, Senior Laboratory Engineer, District 19; Warren N. Dudley, Senior Laboratory Engineer, District 20; and Gaston P. Berthelote, Jr., Supervising Resident Engineer, Houston Urban Project, whose cooperation in providing field assistance and basic information made the success of this investigation possible.

The able assistance of various members of the Research Section, Ivan K. Mays, and others who were instrumental in the success of this investigation, is gratefully acknowledged. The field party that gathered the data is also to be commended.

REFERENCES

1. Status Report on Continuously Reinforced Concrete Pavement Built or Under Contract in the U.S. Concrete Reinforcing Steel Institute, July 1966.
2. Shelby, M. D., and McCullough, B. F. Experience in Texas With Continuously Reinforced Concrete Pavement. HRB Bull. 274, p. 1-29, 1960.
3. McCullough, B. F., and Ledbetter, W. B. LTS Design of Continuously Reinforced Concrete Pavements. Jour. Highway Div., Proc. ASCE, Vol. 86, No. HW4, Dec. 1960.
4. AASHO Interim Guide for the Design of Rigid Pavement Structures. AASHO Committee on Design, April 1962.
5. The AASHO Road Test: Report 5, Pavement Research. HRB Spec. Rept. 61E, 1962.

6. McCullough, B. F. Development of Equipment and Techniques for a Statewide Rigid Pavement Deflection Study. Research Rept. No. 46-1, Texas Highway Department, Jan. 1965.
7. McCullough, B. F. Evaluation of Single Axle Load Response on an Experimental Continuously Reinforced Concrete Pavement. Research Rept. No. 46-3, Texas Highway Department, April 1965.
8. McCullough, B. F., and Treybig, H. J. Determining the Relationship of Variables in Deflection of Continuously Reinforced Concrete Pavement. Research Rept. No. 46-4, Texas Highway Department, Aug. 1965.
9. Manual of Testing Procedures, Vol. 1. Texas Highway Department.
10. Design Manual for Controlled Access Highways. Texas Highway Department.
11. Standard Specifications for Road and Bridge Construction. Texas Highway Department, 1962.
12. Hudson, W. R. Value of Single Load Response in Rigid Pavement Design. Paper presented at Texas Section ASCE, May 10, 1963.
13. Taylor, Donald W. Fundamentals of Soil Mechanics (Ninth Printing). John Wiley and Sons, New York, 1956, p. 381-392.
14. McCullough, B. F., and Mays, Ivan K. A Laboratory Study of the Variables That Affect Pavement Deflection. Research Rept. No. 46-6, Texas Highway Department, Aug. 1966.
15. Snedecor, George W. Statistical Methods. Iowa State College Press, Ames, 1946, p. 351.
16. Westergaard, H. M. Stresses in Concrete Pavements Computed by Theoretical Analysis. Public Roads, Vol. 7, No. 2, April 1926.

Editor's Note: The original paper contained six Appendixes pertaining to equipment used, experimental procedure, summaries of data, deflection analysis, and soil support. This material is available from the Highway Research Board at cost of reproduction. When ordering, refer to XS-18, Highway Research Record 239.